2009

An H-Adaptive Finite-Element Technique for Constructing 3D Wind Fields

Darrell Pepper
University of Nevada, Las Vegas, darrell.pepper@unlv.edu

Xiuling Wang
Purdue University Calumet, wangx@calumet.purdue.edu

An *h*-Adaptive Finite-Element Technique for Constructing 3D Wind Fields

DARRELL W. PEPPER

Nevada Center for Advanced Computational Methods, University of Nevada, Las Vegas, Las Vegas, Nevada

XIULING WANG

Purdue University Calumet, Calumet, Indiana

(Manuscript received 2 January 2007, in final form 22 July 2008)

ABSTRACT

An *h*-adaptive, mass-consistent finite-element model (FEM) has been developed for constructing 3D wind fields over irregular terrain utilizing sparse meteorological tower data. The element size in the computational domain is dynamically controlled by an a posteriori error estimator based on the L_2 norm. In the *h*-adaptive FEM algorithm, large element sizes are typically associated with smooth flow regions and small errors; small element sizes are attributed to fast-changing flow regions and large errors. The adaptive procedure employed in this model uses mesh refinement–unrefinement to satisfy error criteria. Results are presented for wind fields using sparse data obtained from two regions within Nevada: 1) the Nevada Test Site, located approximately 65 mi (1 mi ≈ 1.6 km) northwest of Las Vegas, and 2) the central region of Nevada, about 100 mi southeast of Reno.

1. Introduction

Constructing 3D wind fields is important in weather forecasting, wind energy assessment, wind turbine siting, and atmospheric dispersion assessments. However, generating accurate (or realistic) 3D wind fields can be difficult. The primary reason is that measurements of atmospheric flow are generally sparse and insufficient to resolve important flow phenomena. Linking meteorological data with numerical approaches is fairly routine, and has been employed for many years. The majority of numerical models used in meteorological simulations is based on finite-difference or finite-volume techniques, principally because of their simplicity and ease of implementation. More recently, these techniques have adopted the use of unstructured meshes, as compared with the global transformation techniques used many years ago. Over the past 20 years, the finite-element method has begun to become more frequently used for atmospheric simulations. The reasons for its increasing popularity stem back to its intrinsic abilities to deal with complex geometrical problems with inhomogeneous or variable properties, the use of general purpose algorithms, and significant computational enhancements to reduce storage and speed up solutions (Heinrich and Pepper 1999).

The use of local adaptation within the finite-element framework has become one of the most powerful numerical tools currently being employed in many computational fluid dynamics commercial codes. The method has been shown to provide accurate simulation results with minimal computational overhead and cost. This benefit is especially valuable in atmospheric calculations where massive problem domains require computational effort that can easily exceed a computer's resources (Wang and Pepper 2007a). This problem can be particularly troublesome when attempting to create realistic 3D wind fields using a fine enough mesh to accurately capture important terrain features.

Mass consistent models for creating 3D winds have been used over many years and have been found to be effective for modeling atmospheric dispersion as well as for wind energy assessment studies. Such modeling techniques are discussed in Lange (1978), Sherman (1978), Goodin et al. (1980), Pepper (1991), Ratto et al. (1994), Finardi et al. (1998), and Montero and Sanin (2001). The problems stemming from these early applications

Corresponding author address: Darrell W. Pepper, Department of Mechanical Engineering, University of Nevada, Las Vegas, 4505 Maryland Parkway, Las Vegas, NV 89154-4027.
E-mail: dwpepper@nscee.edu

DOI: 10.1175/2008JAMC1680.1

deal with the coarse meshes and inability to deal effectively with refinement where terrain and/or velocities vary dramatically. The application of a mass consistent approach essentially poses a least squares problem in the computational domain (i.e., minimizing the differences between observed and adjusted values).

In this study, two simulations are presented using an *h*-adaptive finite-element model (FEM). In both cases, initial meshes were generated from digital elevation map (DEM) data, developed by the U.S. Geological Survey (USGS). In the first case, a 3D wind field is constructed for the Nevada Test Site (NTS). Numerical results were validated using meteorological data recorded in 1993 from 15 towers. In the second case, a 3D wind field is constructed for the central Nevada region using results from four meteorological towers—a much sparser dataset; this region is being examined for possible wind energy potential (Pepper and Wang 2007). Results are compared with model output from the fifth-generation Pennsylvania State University–National Center for Atmospheric Research (NCAR) Mesoscale Model (MM5) using NCAR's reanalysis data; however, much higher resolution is achieved. In the *h*-adaptation scheme employed in this study, resolutions from kilometers down to meter levels (or smaller, if warranted) can be achieved. When compared with the use of globally uniform and refined meshes for reaching the same levels of accuracy, the *h*-adaptive scheme is significantly more computationally effective and efficient (Wang and Pepper 2007b).

2. Numerical modeling

The diagnostic mass-consistent model is derived from the continuity equation and incorporation of actual field data. The term ''diagnostic'' was used by Pielke (1984) to discuss different mesoscale meteorological models. Early research work on mass-consistent models was undertaken by Sherman (1978) and later applied by Pepper (1991). The main idea of the technique is to match simulation values with measured meteorological data, using weighted averaging around the (usually) sparse data points to fill in values to all the nodes within the computational domain.

A surface wind field is constructed from measured data by interpolation over the initial mesh using inverse-squared weighting ($1/r^2$, where r is the radial distance between the grid points and the tower locations). A fixed radius R is specified, which indicates the distance beyond which the influence of a station's value is no longer felt (Goodin et al. 1979; Kitada et al. 1983; Pepper 1991). Two values were evaluated for R: $R = L/N$ and $R = L$, where L is the length of the horizontal region and N is the number of observations. The use of the former $R = L/N$ provided better results in the evaluation of field data (Goodin et al. 1979; Kitada et al. 1983).

The velocity at a grid point within an upper layer is calculated using the velocity at the grid point that has the same horizontal level as the tower layer. The top-layer velocity is obtained using log-linear interpolation.

Vertical wind velocity is not a commonly observed variable in meteorology and its estimation appears as one of the more difficult problems for modeling studies. The vertical velocity is an integral component in many diagnostic and prognostic problems. In this study, vertical velocities are calculated at all grid points from the equation of continuity using the horizontal wind observations and accounting for the divergence correction, that is,

$$w = -\int_0^z \left(\frac{\partial u}{\partial x} + \frac{\partial v}{\partial y}\right) dz, \tag{1}$$

where u, v, and w are velocities in x, y, and z directions.

Mass-consistent FEM

The finite-element method is a popular numerical technique that has been used to solve structural problems in engineering since its inception in the mid-1950s. Application of the FEM to other fields, particularly fluid flow, began to occur around the late 1970s (Zienkiewicz and Zhu 1987) and has continued to mature over the years.

In comparison with finite-difference methods, the finite-element method is more attractive in its capability to deal with complex geometries. In finite-difference and finite-volume methods commonly used in the past, the mesh consisted of rows and columns of orthogonal lines (in computational space, a requirement now handled through coordinate transformations and unstructured mesh generators); in finite elements, each subdivision is unique and does not need to be orthogonal (Pepper and Heinrich 2006). The finite-difference approach utilizes the discretization of variables and gradient terms based upon Taylor series approximation and nodal molecules (usually three-point approximations yielding second-order spatial accuracy in each direction). The FEM is based on application of the method of weighted residuals stemming from Galerkin's integral approach, and minimizes error throughout the computational domain. By utilizing basis functions to approximate spatial distances (via elements instead of node point intervals), the FEM permits one to capitalize on a family of interpolations that can yield much higher spatial accuracies.

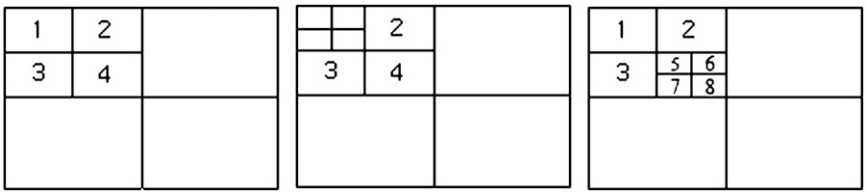

FIG. 1. Example for *h*-adaptation.

For example, in the finite-element method,[1] an unknown variable (velocity, temperature, etc.) is approximated using known functions (termed shape functions) over each discretized element. In contrast to finite-difference procedures, the governing equations in the finite-element method are integrated over each finite-element and the contributions summed ("assembled") over the entire problem domain. As a consequence of this procedure, a set of finite linear equations is obtained in terms of the set of unknown parameters over the elements. Solutions of these equations are achieved using linear algebra techniques (the matrices are usually sparse but they can be efficiently solved).

Generally, in FEM, there are two ways to increase computational accuracy—use a fine mesh (refinement) or apply higher-order approximation (enrichment). Since atmospheric calculations usually require large computational resources, it is typically impractical to use a uniform fine mesh or higher-order approximations over the entire computational domain. Fortunately, adaptive FEM allows one to use local refinement (*h*-adaptation) or local enrichment (*p*-adaptation), thereby significantly reducing storage and computational time when compared to globally refined or enriched meshes (see Wang and Pepper 2007a,b).

A 3D mass-consistent model was first used to generate wind fields for the Atmospheric Diffusion Particle-in-Cell (ADPIC) pollutant transport model developed at Lawrence Livermore National Laboratory by Lange (1978). Early research work was conducted by Sherman (1978), who developed a mass-consistent model for wind fields over complex terrain, and Dickerson (1978), who developed the mass-consistent atmospheric model for regions with complex terrain. The basis of their technique stems back to an objective analysis approach using a Sasaki variational technique (Sasaki 1958). This technique was later applied by Mathur and Peters (1990) for application in air pollution modeling and by Pepper (1991) using a FEM approach to predict meso-scale wind fields over Vandenberg Air Force Base. Montero et al. (2005) developed genetic algorithms for improved parameter estimation with local tetrahedral mesh refinement in a wind model. The selection of parameters and computational methods implemented by different mass consistent models is discussed by Ratto et al. (1994). We elected to use this approach in lieu of other techniques because of its simplicity and ease of implementation with adaptivity. Warner et al. (1983) describes the use of observed winds versus predicted winds employing a 3D dynamic model to predict medium-range atmospheric transport, along with shortcomings in accuracies attributed to each technique. Schaefer and

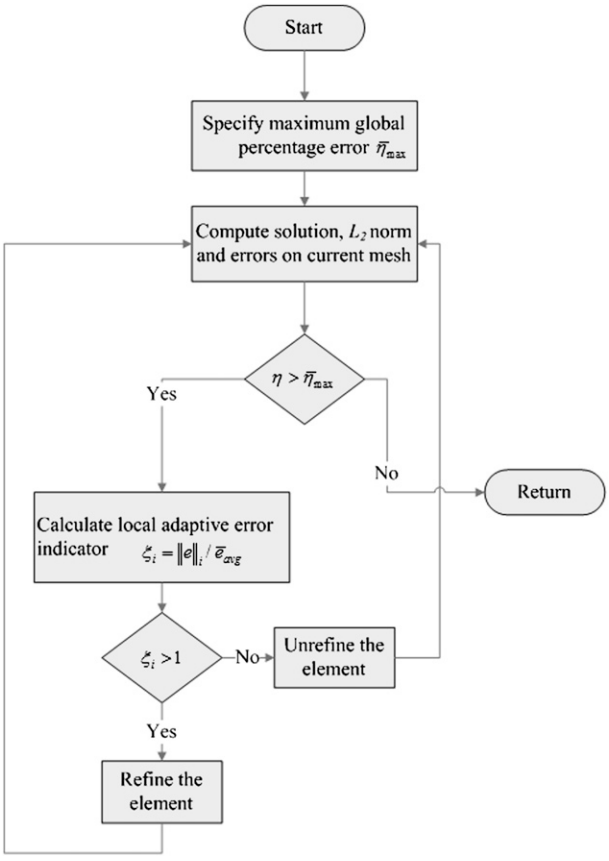

FIG. 2. Flowchart for *h*-adaptation procedure.

[1] Readers unfamiliar with the details of the finite-element method may want to consult the text by Pepper and Heinrich (2006) for additional information.

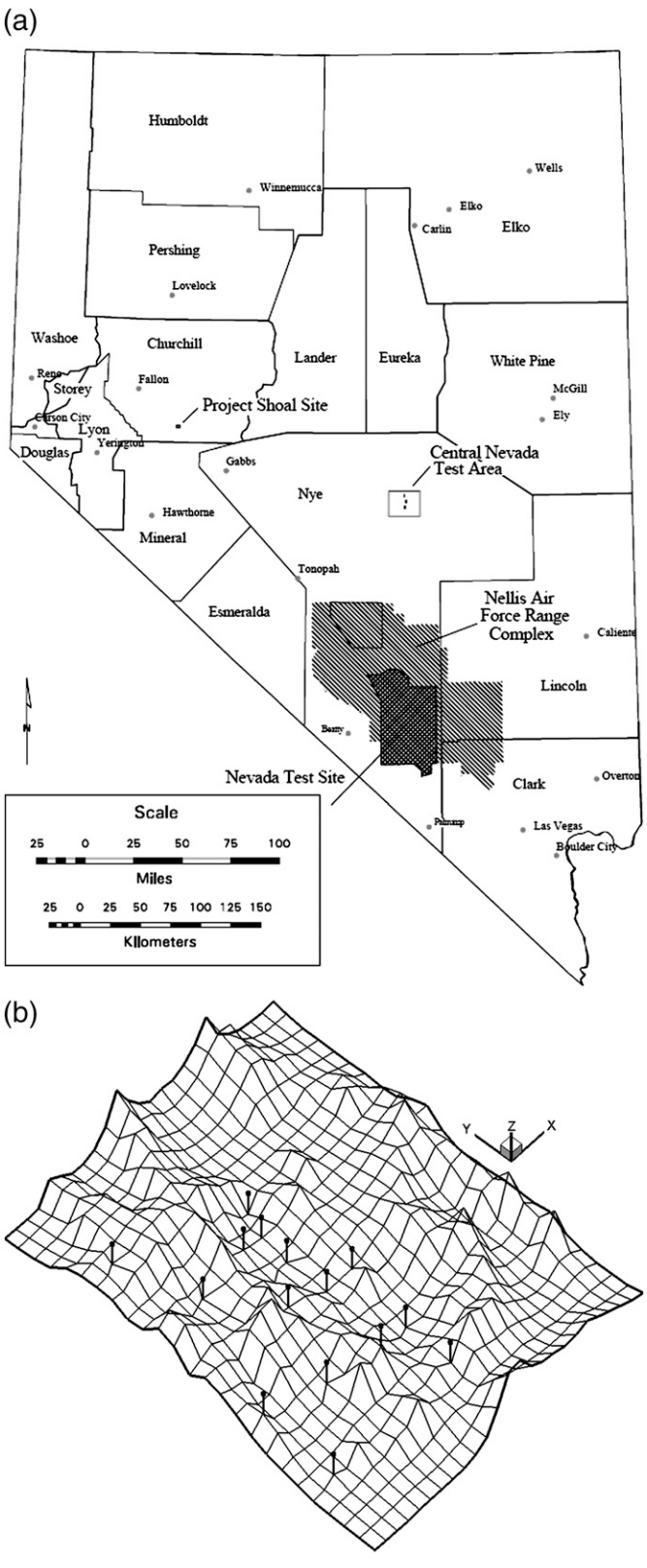

FIG. 3. (a) NTS and (b) tower locations.

TABLE 1. Tower locations for NTS.

Tower no.	Lat	Lon	Elev (m)
2	37°8′21″	116°6′21″	1341
5	36°48′6″	115°58′0″	942
6	36°57′30″	116°2′48″	1195
9	37°8′9″	116°2′24″	1289
11	36°57′12″	115°57′33″	1256
14	36°58′3″	116°10′27″	1436
15	37°11′24″	116°1′9″	1362
17	37°3′45″	116°3′9″	1244
18	37°6′9″	116°18′33″	1536
20	37°15′21″	116°26′6″	2003
23	36°39′30″	115°59′45″	1140
24	36°49′36″	116°27′57″	1183
25	36°40′30″	116°24′48″	838
26	36°48′39″	116°15′0″	1140
27	36°46′12″	116°6′15″	1381

Doswell (1979) discuss issues attributed to the interpolation of a vector field for atmospheric simulations; their analysis was based on finite differences and regional scales.

In this model, an Euler–Lagrange method is used in an integral function that minimizes the variance of the difference between the observed and analyzed variables (Sasaki 1958). The function can be written as

$$E(u,v,w,\lambda) = \int_\Omega \left[\alpha_1^2(u-u_0)^2 + \alpha_1^2(v-v_0)^2 + \alpha_2^2(w-w_0)^2 + \lambda\left(\frac{\partial u}{\partial x} + \frac{\partial v}{\partial y} + \frac{\partial w}{\partial z}\right)\right] d\Omega, \tag{2}$$

where u_0, v_0, and w_0 are observed velocity values in x, y, and z direction, Ω is the physical domain ($d\Omega \equiv dxdydz$), and α_i are Gauss precision moduli, where $\alpha_i^2 \equiv 1/2\sigma_i^2$ (σ_i are observation tower errors and/or deviations of the observed field from the desired adjusted field). For horizontal directions, the Gauss precision moduli are assumed identical, since apparent distinctions exist between horizontal and vertical directions, but not between x and y coordinates (see Sherman 1978). These moduli are important in determining the nondivergence wind field over irregular terrain. Sherman (1978) suggested that $(\alpha_1/\alpha_2)^2$ should be proportional to the magnitude of the expected $(w/u)^2$. Using this relation and studies from Kitada et al. (1983), the 3D flow fields tested for the minimum residual divergence occurred at about $(\alpha_1/\alpha_2)^2 = 0.01$. In this study, the values of α_1 and α_2 were taken to be 0.01 and 0.1, respectively.

The corresponding Euler–Lagrange equations whose solutions minimize Eq. (2) are given as (see Sherman 1978; Kitada et al. 1983; Pepper 1991; Ratto et al. 1994)

$$u = u_0 + \frac{1}{2\alpha_1^2}\frac{\partial \lambda}{\partial x}, \tag{3}$$

$$v = v_0 + \frac{1}{2\alpha_1^2}\frac{\partial \lambda}{\partial y}, \quad \text{and} \tag{4}$$

$$w = w_0 + \frac{1}{2\alpha_2^2}\frac{\partial \lambda}{\partial z}, \tag{5}$$

where λ is the Lagrange multiplier. Substituting Eqs. (3)–(5) into the continuity equation (assuming air density is constant in the computational domain),[2]

$$\frac{\partial u}{\partial x} + \frac{\partial v}{\partial y} + \frac{\partial w}{\partial z} = 0. \tag{6}$$

A Poisson equation for $\lambda(x, y, z)$ can then be obtained of the form

$$\frac{\partial^2 \lambda}{\partial x^2} + \frac{\partial^2 \lambda}{\partial y^2} + \left(\frac{\alpha_1}{\alpha_2}\right)^2 \frac{\partial^2 \lambda}{\partial z^2} = -2\alpha_1^2\left(\frac{\partial u_0}{\partial x} + \frac{\partial v_0}{\partial y} + \frac{\partial w_0}{\partial z}\right). \tag{7}$$

The ratio of α_1/α_2 allows one to adjust between horizontal or vertical influential preference.

Applying the Galerkin method of weighted residuals, the integral form of Eq. (7) can be written as

$$\int_\Omega N_i\left[-\frac{\partial^2 \lambda}{\partial x^2} - \frac{\partial^2 \lambda}{\partial y^2} - \left(\frac{\alpha_1^2}{\alpha_2^2}\right)\frac{\partial^2 \lambda}{\partial z^2} - 2\alpha_1^2\left(\frac{\partial u_0}{\partial x} + \frac{\partial v_0}{\partial y} + \frac{\partial w_0}{\partial z}\right)\right] d\Omega = 0, \tag{8}$$

where N_i is the shape function. The matrix equivalent form of this equation is

$$\mathbf{K}\lambda = \mathbf{f}, \tag{9}$$

where $\mathbf{K}$ is the stiffness matrix

$$\mathbf{K} = \int_\Omega \left(\frac{\partial N_i}{\partial x}\frac{\partial N_j}{\partial x} + \frac{\partial N_i}{\partial y}\frac{\partial N_j}{\partial y} + \frac{\alpha_1^2}{\alpha_2^2}\frac{\partial N_i}{\partial z}\frac{\partial N_j}{\partial z}\right) d\Omega \tag{10}$$

and $\mathbf{f}$ is the load vector (or right-hand side of the equation)

$$\mathbf{f} = 2\alpha_1^2 \int_\Omega N_i\left(\frac{\partial u_0}{\partial x} + \frac{\partial v_0}{\partial y} + \frac{\partial w_0}{\partial z}\right) d\Omega. \tag{11}$$

[2] Since the velocities are low in this case, we assumed a constant density; however, variable density can be added to account for vertical temperature variation if warranted (see Sherman 1978).

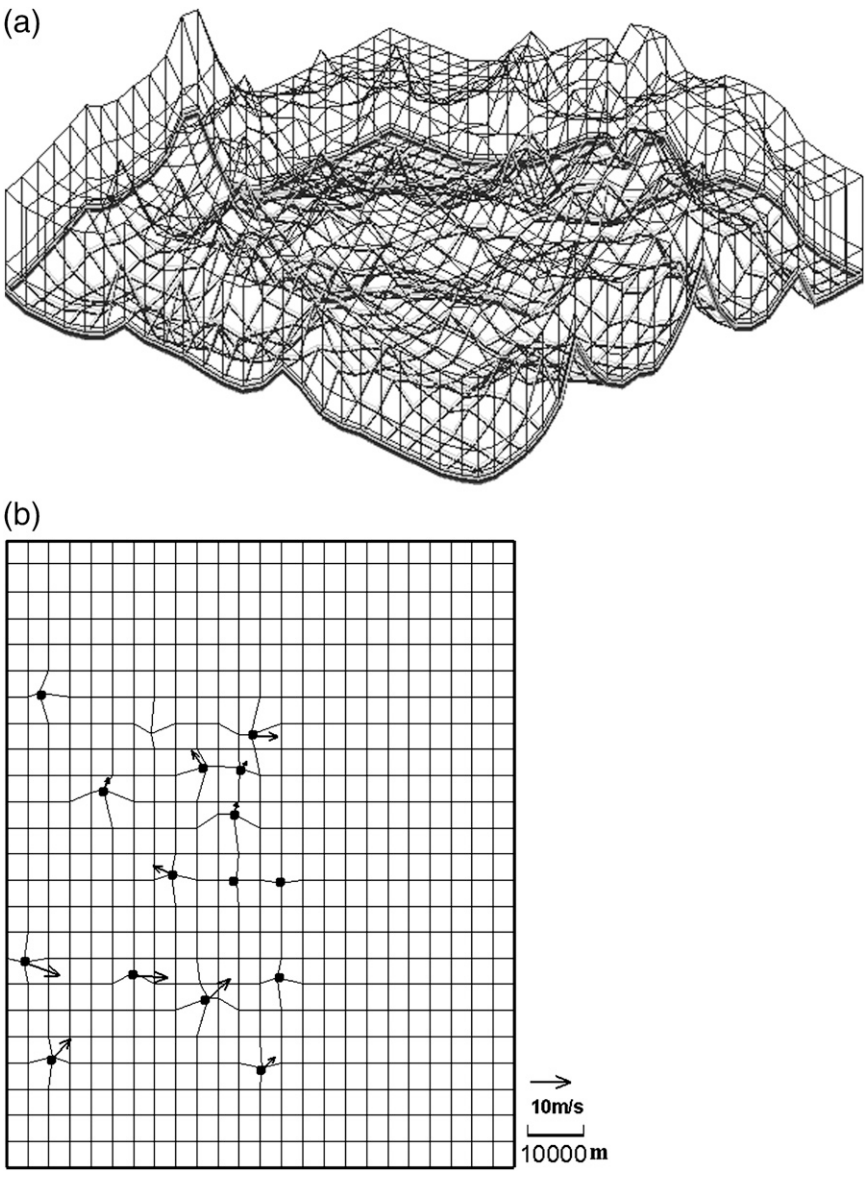

FIG. 4. Initial computational mesh for NTS with averaged wind velocity vectors at each tower location: (a) 3D and (b) 2D view.

The gradient $\partial\lambda/\partial n$ in general is not zero and adjustment of the observed velocities from Eqs. (3)–(5) can be obtained. A nonzero adjustment of the velocity normal to the boundary implies mass entering or leaving the volume. The boundary condition $\lambda = 0$ is appropriate for open or ''flow through'' boundaries.

When $\partial\lambda/\partial n = 0$ on the boundary, the adjusted values of the normal velocity are the same as the observed value. Setting $\partial\lambda/\partial n = 0$ on the boundary does not affect the normal velocity on the boundary. If the observed normal velocity is zero, there will be no transport of mass through the boundary. Therefore, $\partial\lambda/\partial n = 0$ is used for closed or ''no flow-through'' boundaries.

The diagnostic procedure produces a mass consistent wind field that is realistic and fairly accurate that can then be refined to account for microscale topographic flow features. It should be pointed out that Sherman (1978) and Dickerson (1978) found that the use of this particular technique was within a factor of 2 around 50% of the time and within an order of magnitude about 90% of the time. They used a fairly coarse mesh density at the time of their results. We wish to emphasize that the application of adaptation, as a minimum, can provide more detailed visualization and help in assessing the dynamics of the flow.

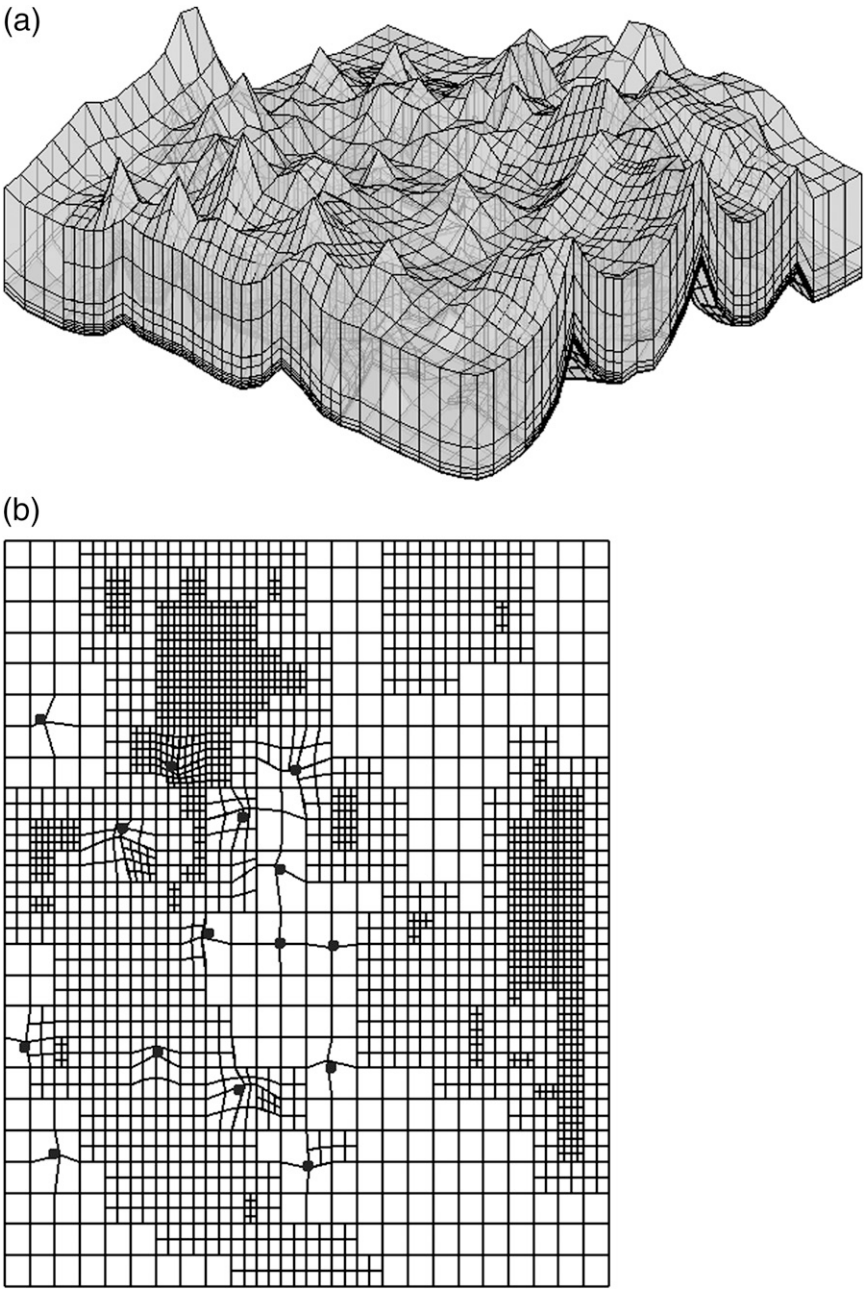

FIG. 5. As in Fig. 4, but for adaptive computational mesh.

3. Adaptive methodology

Adaptive FEM techniques are typically categorized as belonging to one of four procedures: *h-, p-, r-* and *hp*-adaptation. In *h*-adaptation, element size varies while the order of the shape function remains constant; in *p*-adaptation, element size is constant while the order of the shape function is increased to meet the desired accuracy requirement; in *r*-adaptation, the spring analogy is used to redistribute the nodes in an existing mesh; in *hp*-adaptation, both *h*- and *p*-adaptation are combined, resulting in a procedure that is exponentially convergent (Guo and Babuska 1986a,b).

The advantage of using *h*-adaptation is that the elements are kept from being overly distorted; the disadvantage is the complexity of the adaptation algorithm due to constraint (or virtual) nodes when dealing with quadrilateral or hexahedral elements (Demkowicz et al.

TABLE 2. Wind speed records of NTS towers on 1 Jan 1993. The units are meters per second for r, U, and V, and degrees for θ.

Time (LT)	0100		0115		0130		0145		Avg	
Tower no.	r	θ	r	θ	r	θ	r	θ	U	V
2	6	313	7	311	6	319	6	13	−3.07	4.76
5	1	336	1	273	3	156	1	134	0.13	−0.62
6	1	359	1	193	1	348	3	348	−0.27	−0.98
9	3	31	4	9	4	15	3	102	1.53	2.44
11	1	103	2	151	1	96	2	23	0.93	−0.059
14	6	295	7	296	6	295	5	296	−5.42	2.57
15	3	43	7	95	7	98	9	103	6.18	−0.35
17	4	356	3	17	5	18	3	355	0.46	3.65
18	5	12	4	18	4	24	4	14	1.22	4.06
20	1	161	1	152	1	147	1	158	0.43	−0.90
23	4	65	6	37	5	49	4	28	3.22	3.32
24	10	107	10	108	9	115	9	11	8.91	−3.25
25	7	33	8	38	8	50	7	44	4.93	5.59
26	8	92	10	97	9	85	10	98	9.20	−0.52
27	9	38	9	37	8	56	8	65	6.21	5.54

1989). The advantage of using r-adaptation is that the number of elements can be kept constant; the disadvantage is that the elements may become overly distorted. The major advantage of p-adaptation is the enhanced accuracy improvements using only a coarse mesh; however, the disadvantage is the complexity associated with development of the program. While hp-adaptation is the best method with regards to overall accuracy and speed of convergence, the bookkeeping and program logic can be quite complicated; early efforts to utilize hp-adaptation appear promising and are reported by Wang and Pepper (2007a,b).

The h-adaptation is especially promising in atmospheric simulations where regions with fast changing flow features occur throughout the computational domain. While the application of mesh adaptation has been in use for many years in both structural and aerospace engineering areas, the use of the technique in environmental applications has been somewhat limited. Pepper and Stephenson (1995) used an h-adaptive FEM for calculating the subsurface transport of contaminant. Winter et al. (1995) investigated adaptive strategies for wind field adjustments using standard and mixed FEM. Pepper and Carrington (1999) used h-adaptive FEM to model environmental flows with species transport. Nithiarasu and Zienkiewicz (2000) used h-adaptive FEM to model general fluid flow problems. Montero et al. (2005) studied the effects of mesh (tetrahedral elements) refinement based on gradients associated with several parameters for the mass-consistent FEM.

In this study, the h-adaptive mass-consistent FEM is controlled by an a posteriori error estimator based on the L_2 norm calculations. Based on the L_2 norm error estimator, the optimal final adaptive mesh (with equally distributed error) can be expected, which is ideal in numerical simulation. The error estimator used in this study is described in more detail in section 3a. Hexahedral elements are used instead of tetrahedral elements in considering anisotropic properties and improved computational accuracy (Biswas and Strawn 1998), although element compatibility becomes an issue.

Various rules must be followed in h-adaptive simulations when dealing with quadrilateral and hexahedral elements. One of the most important rules in h-adaptation is the 1-irregular mesh rule—an element can be refined only if its neighbors are at the same or higher adaptation level (adaptation level relates to how many times it is refined: for the original mesh the adaptation level is labeled 1; if the mesh has been refined once, the adaptation level goes to 2; if the mesh has been refined twice, level 3, etc.). By following this rule, multiple constrained nodes—parent nodes themselves are constraint nodes—can be avoided. A vertex node that lies in the interior of a large element edge, and the two midedge nodes lying on the smaller element edges, are defined as constrained nodes (see Demkowicz 2006). An example is given in Figs. 1a–c of 2D h-adaptation. In Fig. 1a, among the four smaller elements only element 1 can be refined, as its neighbor elements 2 and 3 are at the same adaptation level as element 1. Correct refinement results are shown in Fig. 1b. Element 4 (it is considered a parent element for elements 5–8; the nodes for element 4 are considered parent nodes for those of elements 5–8) cannot be refined since it has neighbor elements with a lower adaptation level. Figure 1c shows an incorrect adaptive mesh for refining element 4, resulting in a two-adaptation-level difference in the final mesh and thus violating the 1-irregular mesh adaptation rule.

Efficient handling of constrained nodes can be troublesome in h-adaptation; a detailed description of the procedure is discussed in Demkowicz et al. (1989).

a. Error estimator

Element sizes in the computational domains examined in this study are dynamically controlled using an a posteriori error estimator. This error estimator is based on the L_2 norm. Large element sizes are usually associated with smooth flow regions and small errors; small element sizes result when there are fast changing flow regions and large errors. Various error estimators exist in the literature (Ainsworth and Oden 2000). The error estimator used in this study is based on an extension of the work by Zienkiewicz and Zhu (1987); a detailed description of the error estimator can also be found in the work by Wang and Pepper (2007a).

The error in velocity can be written as

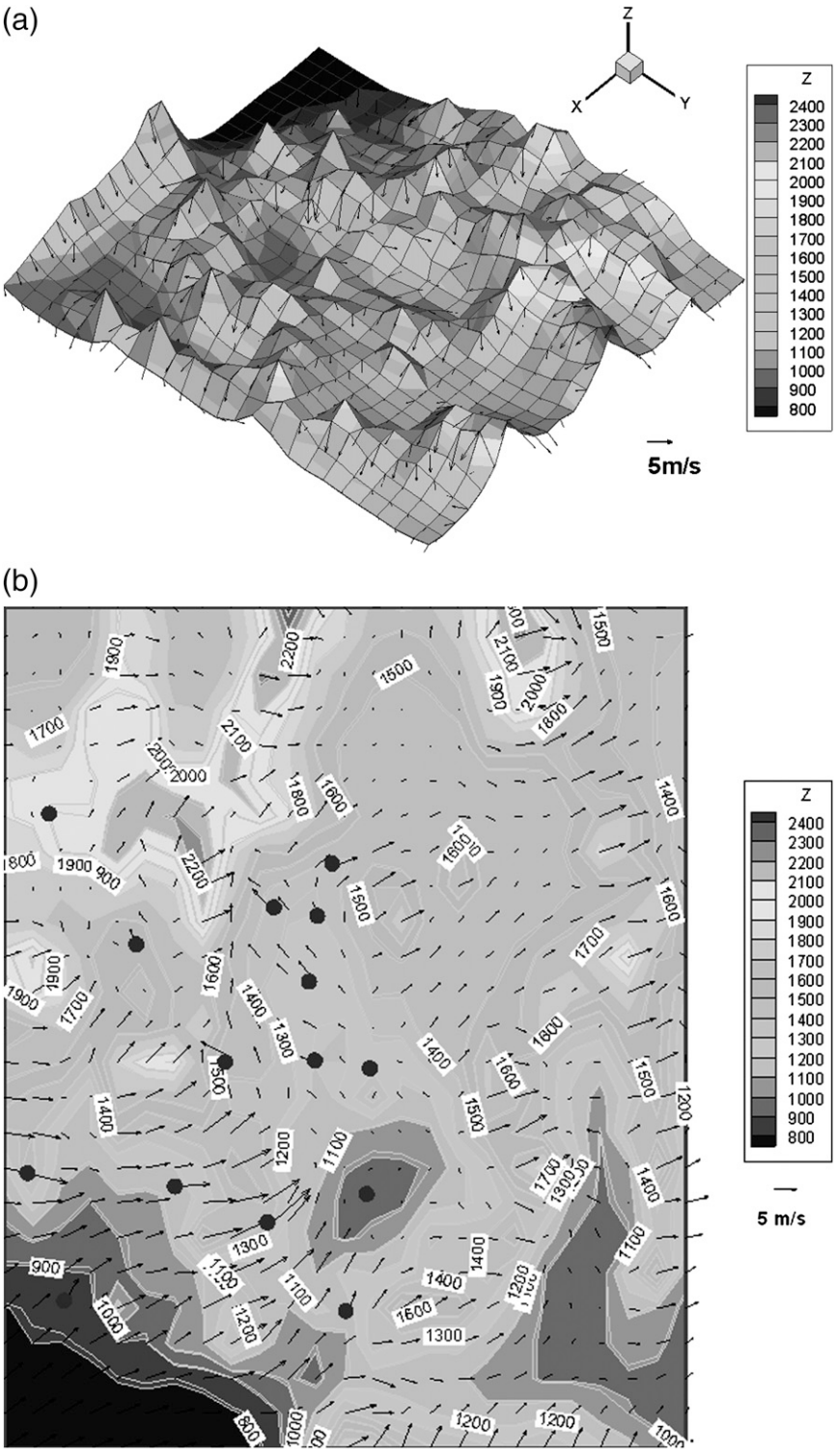

FIG. 6. Wind field at 10 m with topographic contours (without adaptation) for NTS: (a) 3D and (b) 2D view.

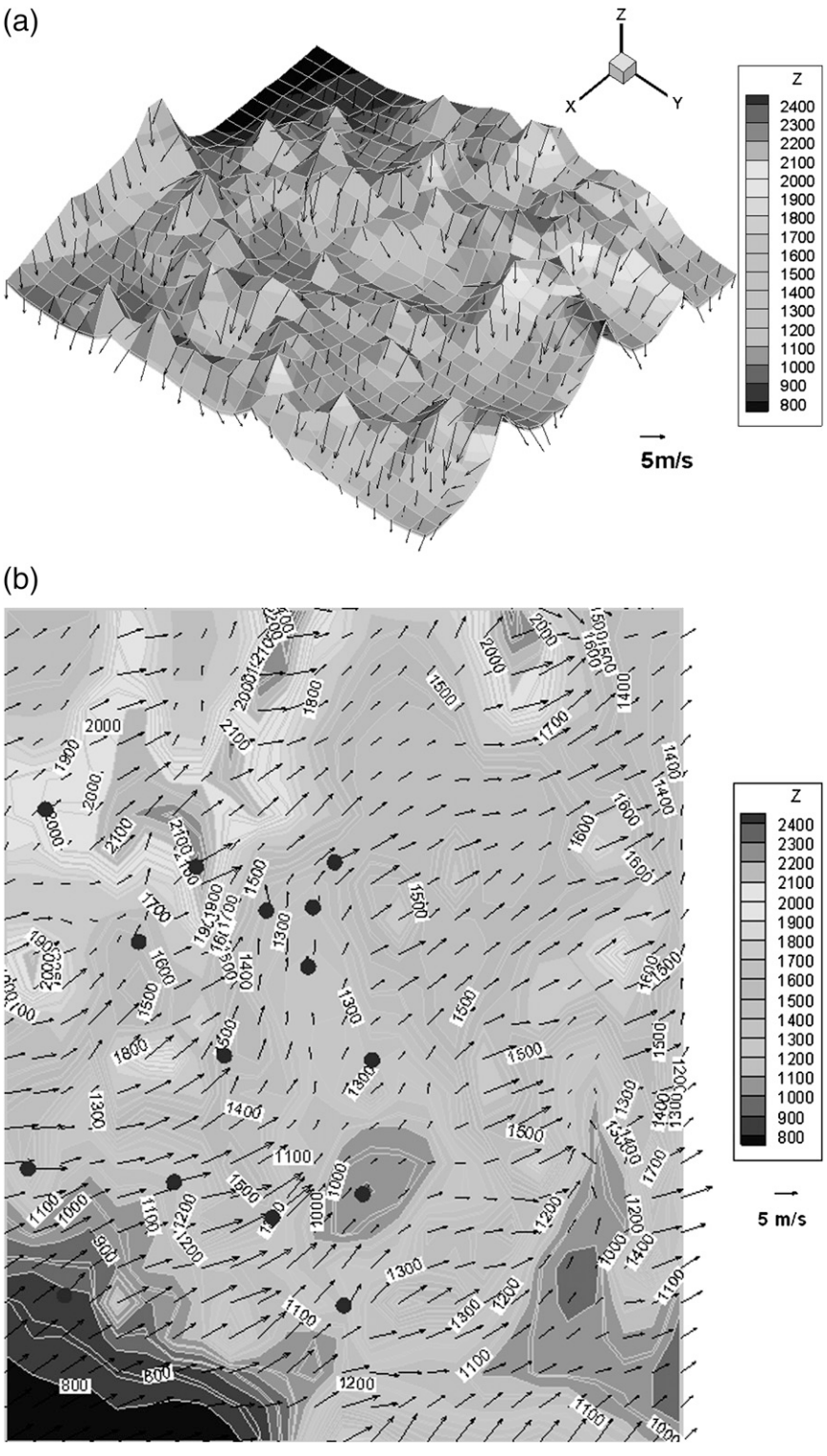

FIG. 7. As in Fig. 6, but for the wind field at 50 m.

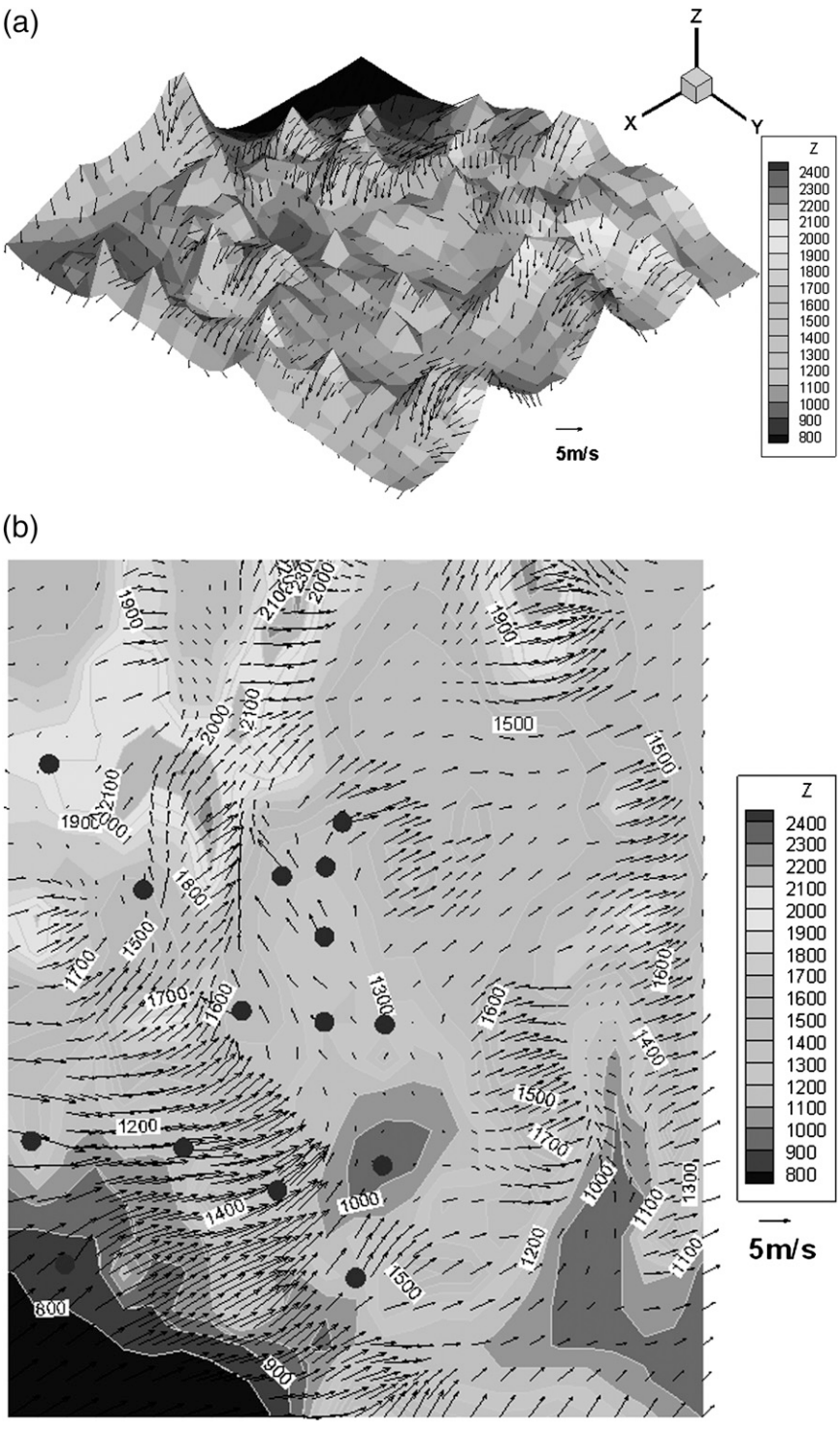

FIG. 8. As in Fig. 6, but with adaptation.

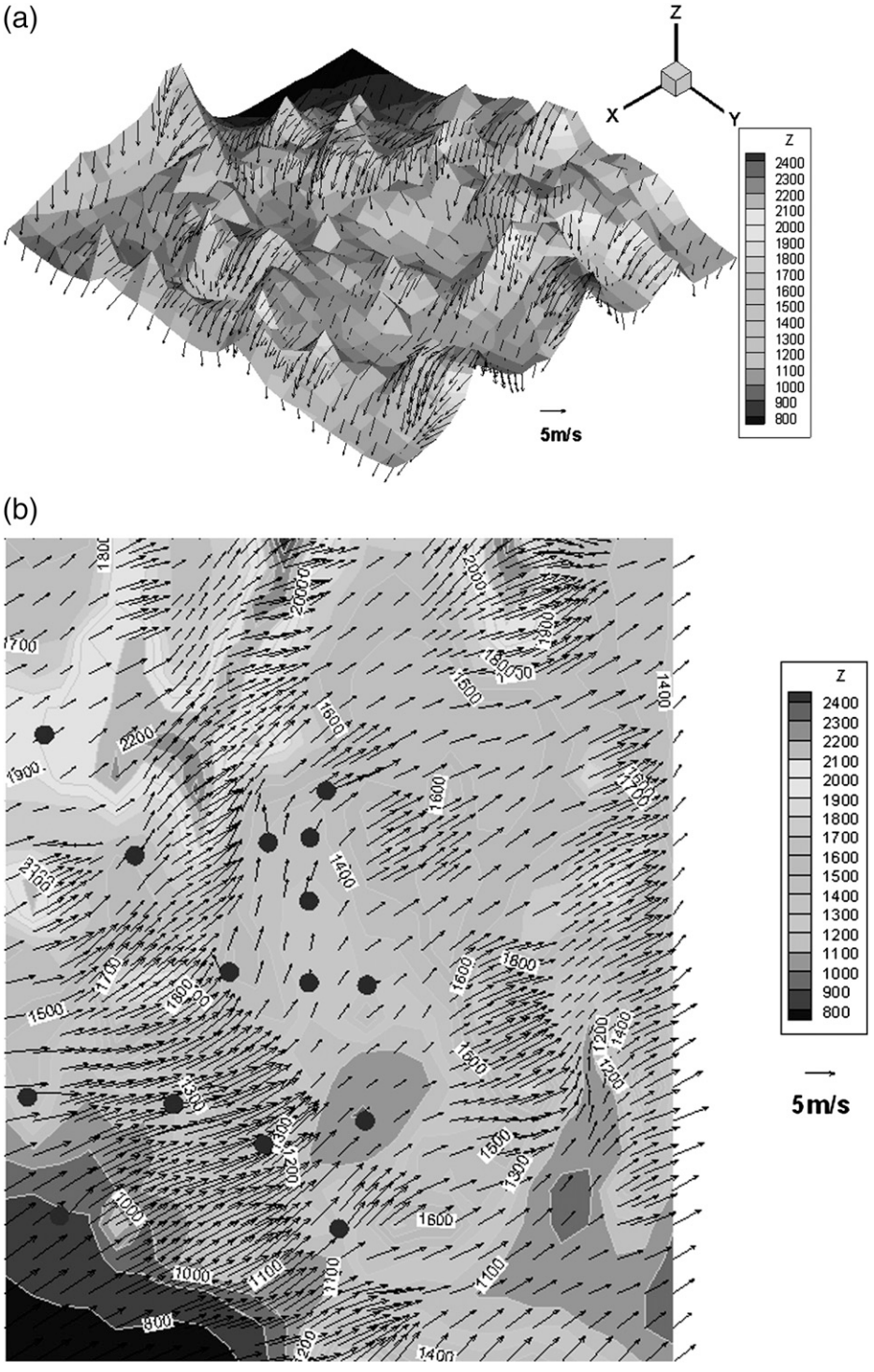

FIG. 9. As in Fig. 7, but with adaptation.

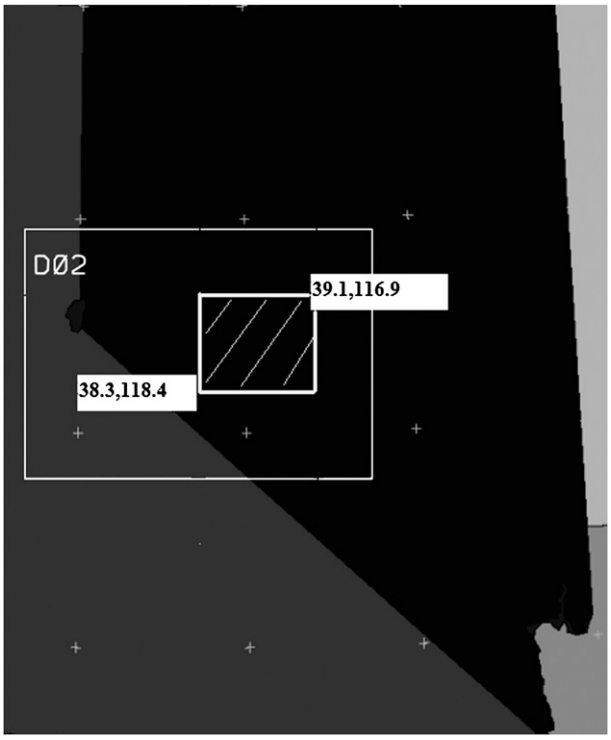

FIG. 10. Computational domain for central Nevada for MM5 and finite-element modeling.

$$\|\mathbf{e}_V\| = \left(\int_\Omega \mathbf{e}_V^{\mathrm{T}}\mathbf{e}_V \, d\Omega\right)^{1/2}, \tag{12}$$

where the superscript T is the transpose. All element errors can be defined as

$$\|\mathbf{e}_V\|^2 = \sum_{i=1}^{m} \|\mathbf{e}_V\|_i^2, \tag{13}$$

where m stands for the total number of elements.

The error index, $\eta = \eta_V$, in the form of the error percentage, can be defined as

$$\eta_V = \left(\frac{\|\mathbf{e}_V\|^2}{\|\mathbf{V}^*\|^2 + \|\mathbf{e}_V\|^2}\right)^{1/2} \times 100\%. \tag{14}$$

The error index η is used to guide the adaptation procedure. The total velocity (all components) is chosen as one of the key adaptation variables in this study. The $\mathbf{V}^*$ stands for the exact solutions. In most practical problems, exact solutions are unavailable. However, a continuous solution can be obtained using a projection or averaging process (see Zienkiewicz and Zhu 1987).

TABLE 3. Tower locations for central Nevada region.

Site no.	Lat	Lon	Elev (m)
1	39°5′52.97″	117°3′47.36″	1674
2	38°22′19.42″	117°28′17.74″	1540
3	38°34′20.99″	118°10′31.68″	1520
4	38°32′37.39″	118°17′39.91″	1354

In this study, the interpolated results are used as the exact solution (i.e.,$\mathbf{V}^*$).

b. Adaptation strategy

An acceptable solution is reached when global and local error conditions are met (Oñate and Bugeda 1994). The global percentage error should not be greater than a maximum specified percentage error: $\eta \le \overline{\eta}_{\max}$. If $\eta > \overline{\eta}_{\max}$, a new iteration is performed. The local relative percentage error of any single element $|\mathbf{e}_V|_i$ should not be greater than the averaged error $\overline{e}_{\mathrm{avg}}$ among all the elements in the domain. The average element error is defined as

$$\overline{e}_{\mathrm{avg}} = \overline{\eta}_{\max}\left(\frac{\|\mathbf{V}^*\|^2 + \|\mathbf{e}_V\|^2}{m}\right)^{1/2}. \tag{15}$$

A local element refinement indicator is defined to decide if a local refinement for an element is needed, that is,

$$\xi_i = \frac{\|\mathbf{e}\|_i}{\overline{e}_{\mathrm{avg}}}. \tag{16}$$

When $\xi_i > 1$, the element is refined; when $\xi_i < 1$, the element may be unrefined. In an h-adaptive process, the new element size is calculated using

$$h_{\mathrm{new}} = \frac{h_{\mathrm{old}}}{\xi_i^{1/p}}. \tag{17}$$

A flowchart of the entire process is shown in Fig. 2. The definitions for variables appearing in Fig. 2 are the same as described in sections 3a and 3b.

4. Simulation results

Two sets of 3D adaptive mass-consistent wind fields were constructed: one for the Nevada Test Site and the other for a region within central Nevada. Good agreement in velocity magnitude and general direction was achieved for both cases using meteorological tower data and MM5 simulations.

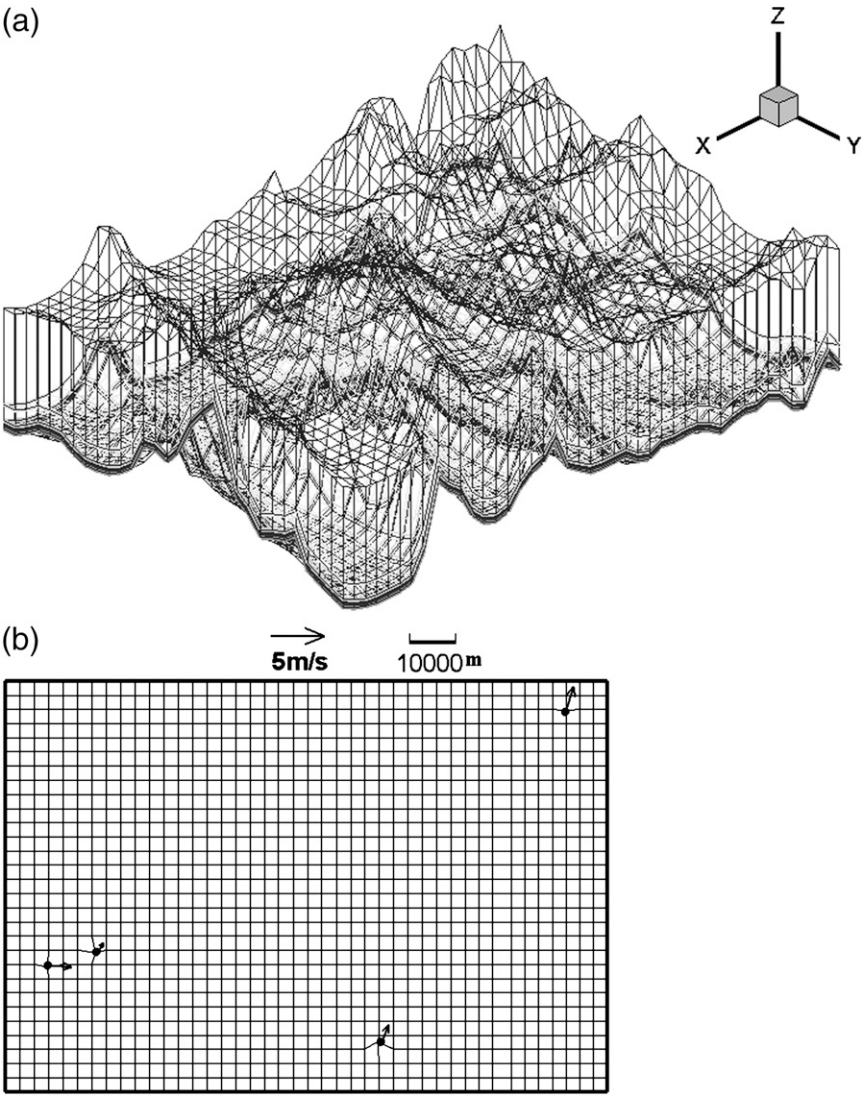

FIG. 11. Initial computational mesh for central Nevada along with initial wind velocity vectors at tower locations: (a) 3D and (b) 2D view.

a. 3D adaptive wind fields for Nevada Test Site

The NTS is a massive outdoor laboratory established in 1950 as the U.S. continental nuclear weapons testing area. The location of the NTS is shown in Fig. 3a, near the southern part of Nevada and beginning about 65 mi (1 mi $\approx$ 1.6 km) northwest of Las Vegas. The NTS is defined by west longitudes 115.5°–116.5° and north latitudes 36.5°–37.5°. A total of 26 (currently 15 operational) towers were placed within the NTS to support nuclear testing in the early 1950s. An unstructured surface mesh with the locations of the towers is shown in Fig. 3b; the exact tower locations are listed in Table 1. A set of four terrain-following layers (10, 50, 300, and 1000 m) was used to construct the initial mesh based on data from the USGS DEM. This initial mesh consisted of 2880 hexahedral elements and 3750 nodes—a 3D view of the mesh is shown in Fig. 4a. In the Fig. 4b 2D view, the tower locations are incorporated as nodal points (denoted by dark dots and marked by tower numbers) within the nonorthogonal mesh.

TABLE 4. Initial velocities from MM5 at 0100 LT 5 Dec 2001 at tower locations for central Nevada region.

Tower	Initial U (m s^{-1})	Initial V (m s^{-1})
1	0.77	2.56
2	0.77	1.83
3	0.62	1.00
4	2.33	−0.16

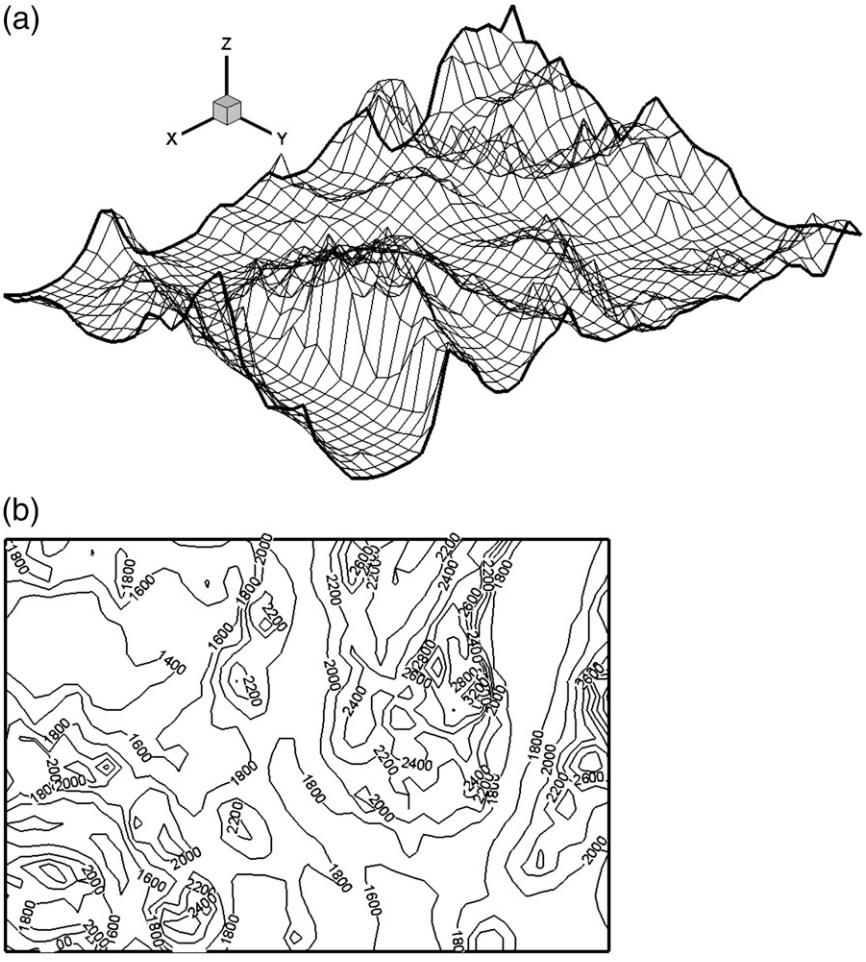

FIG. 12. (a) Terrain surface plot (m) and (b) topographic contours for central Nevada.

A three-level *h*-adapted mesh is shown in Fig. 5. The final adapted mesh consisted of 10 392 elements and 12 508 nodes. The horizontal fine mesh resolution is 950 m.

Three-dimensional, mass-consistent wind fields were constructed with and without adaptation. The recorded averaged measured data for each tower during the time interval from 0100 to 0145 LT 1 January 1993 were used with 15-min intervals. Wind speeds and directions associated with the 15 towers during this period of time are shown in Table 2, where r now refers to the wind speed magnitude (m s^{-1}) and θ refers to the wind direction (the angle between the wind vector and the horizontal direction in counterclockwise direction). The averaged wind velocity vectors at each tower location are shown in Fig. 3a.

Mass-consistent wind fields are shown for the 10- and 50-m levels with and without adaptation in Figs. 6–9. As can be seen, higher-resolution results are obtained by incorporating adaptation into the solution procedure, resulting in a more detailed and realistic 3D wind field near regions where velocities are rapidly changing.

b. 3D adaptive wind fields for central Nevada

The construction of 3D wind fields for the central Nevada region was dictated by the need to conduct a wind energy assessment study for the state. This effort was coordinated between the University of Nevada, Las Vegas (UNLV) and the Desert Research Institute (DRI) at the request of the National Renewable Energy Laboratory, located in Golden, Colorado. Preliminary studies showed that central Nevada could be a good potential region for wind energy. An initial wind field used for finite-element calculation was constructed using the MM5. The MM5 simulations were conducted for an entire year, starting from 1 September 2001 to 31 August 2002. MM5 was initialized from

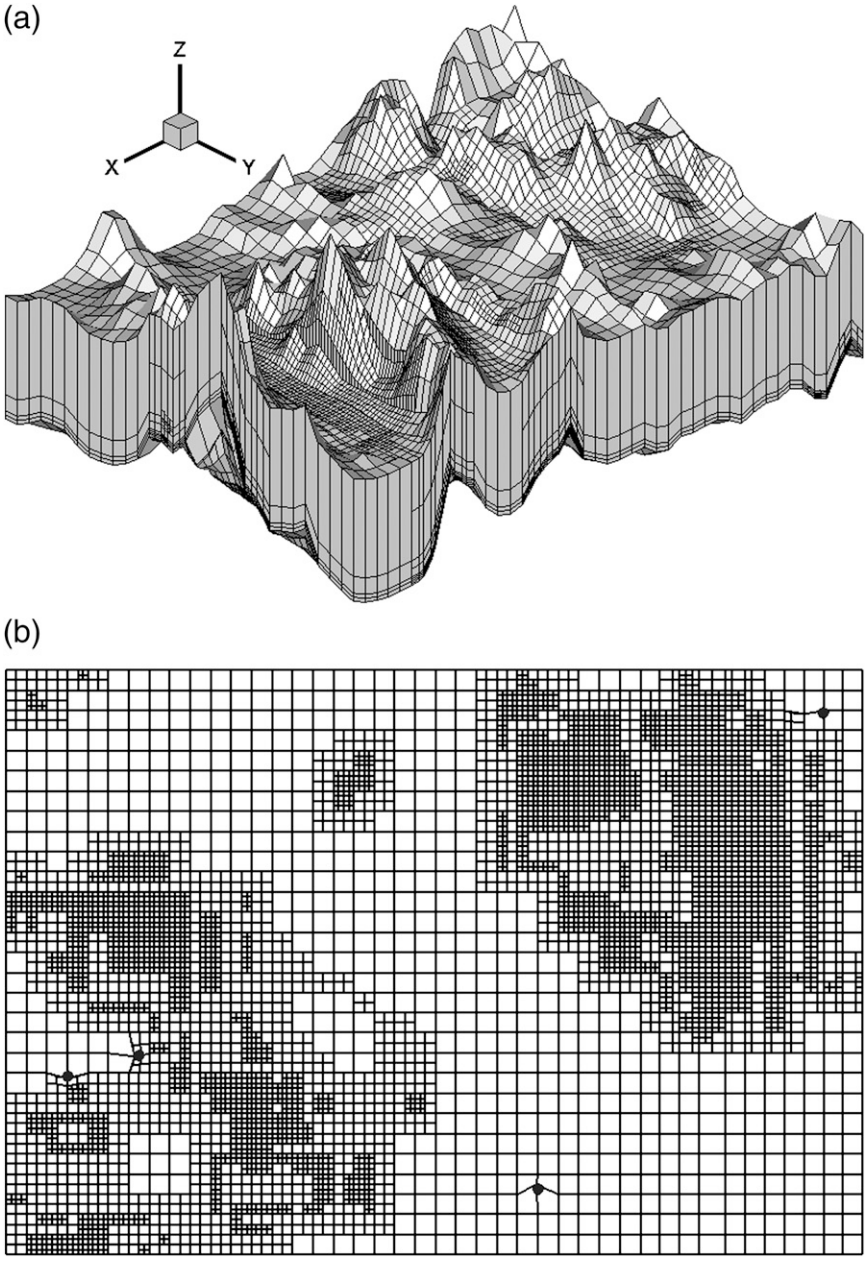

FIG. 13. Adaptive final mesh for central Nevada: (a) 3D and (b) 2D view.

the NCEP Eta Model reanalysis files (NCAR archived dataset 609.2), as well as NCEP ADP upper-air and surface observations (NCAR archived datasets 353.4 and 464.0, respectively). Four-dimensional data assimilation was not used. In addition, the five-layer soil model capability in MM5 was not activated. The first level (vertical height) is approximately 11 m. The MM5 modeling domain is shown in Fig. 10 (grid dimensions are Do1: 120 × 95 × 39; Do2: 118 × 85 × 39). The horizontal resolution is 9 km for domain 1 and 3 km for domain 2 using 39 full sigma levels in the vertical direction. For more information describing the MM5, visit the MM5 Web site (http://www.mmm.ucar.edu/mm5/).

Four 50-m towers were installed at locations that indicated preliminary high potential wind power density profiles. The FEM domain (shown in Fig. 10, marked by the white square) included the four tower locations ranging from 116.9° to 118.4°W longitude and from 38.3° to 39.1°N latitude. Detailed information for

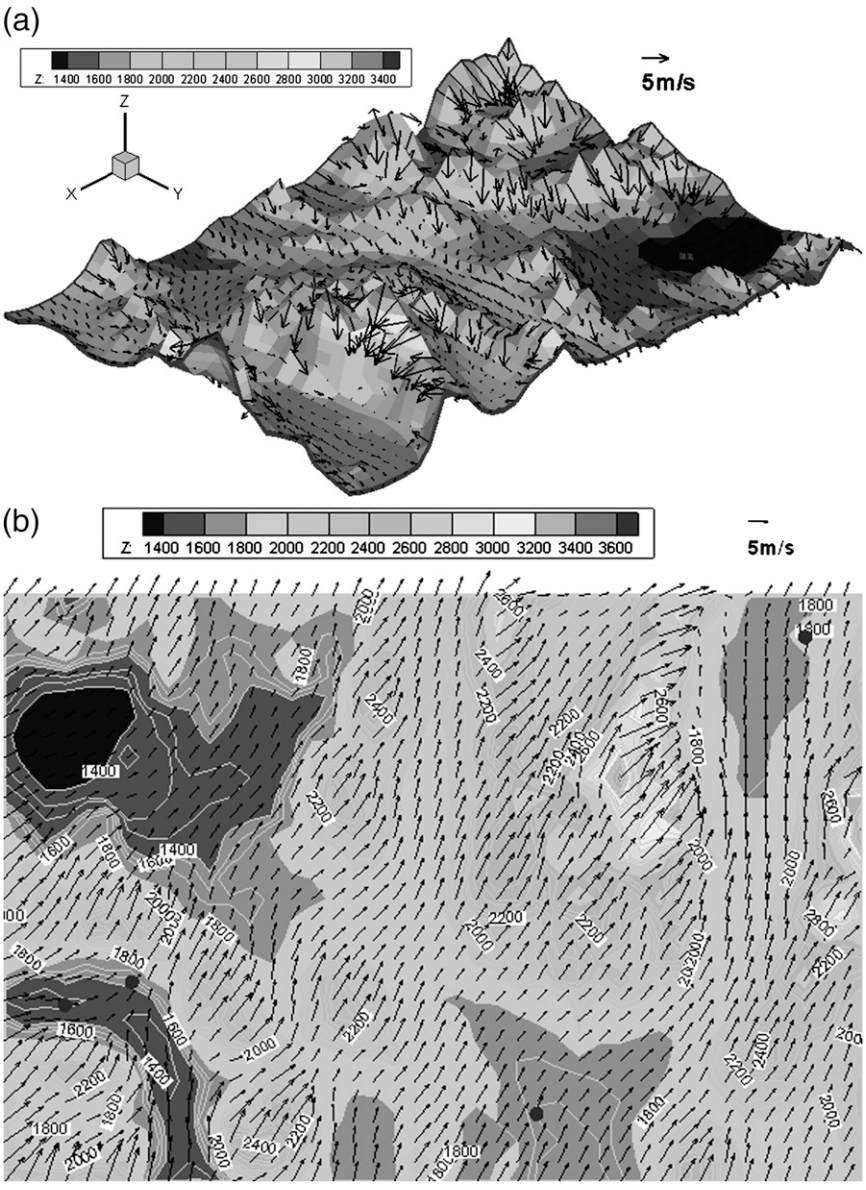

FIG. 14. Wind fields at 100 m with topographic contours (from MM5) for central Nevada: (a) 3D and (b) 2D view.

tower locations is given in Table 3. A terrain-following computational mesh for the FEM was also generated from USGS DEM data.

The initial mesh consisted of five coarse height layers set at 1) surface level, 2) 50-m level, 3) 100-m level, 4) 300-m level, and 5) 1500-m level. Horizontal resolution was set to 3 km for the initial mesh. Both 3D and 2D views of the initial computational mesh are shown in Figs. 11a and 11b; the nonorthogonal, unstructured meshes are shown with tower locations as grid points, which are indicated as dots. Initial tower velocities from MM5 at 0100 LT 5 December 2001 for the central Nevada region are shown in Table 4; the initial wind velocity vectors at tower locations are also shown in Fig. 11b. The initial mesh consisted of 4872 elements and 6450 nodes.

Figures 12a and 12b show the terrain surface plot and topographic contours, respectively; the units for the elevation are in meters.

For demonstrative purposes, wind fields at 0100 LT 5 December 2001 are shown for both the MM5 simulation and the adaptive FEM results. The final three-level, *h*-adaptive mesh consisted of 45 136 elements and 59 482 nodes. The horizontal resolution for the

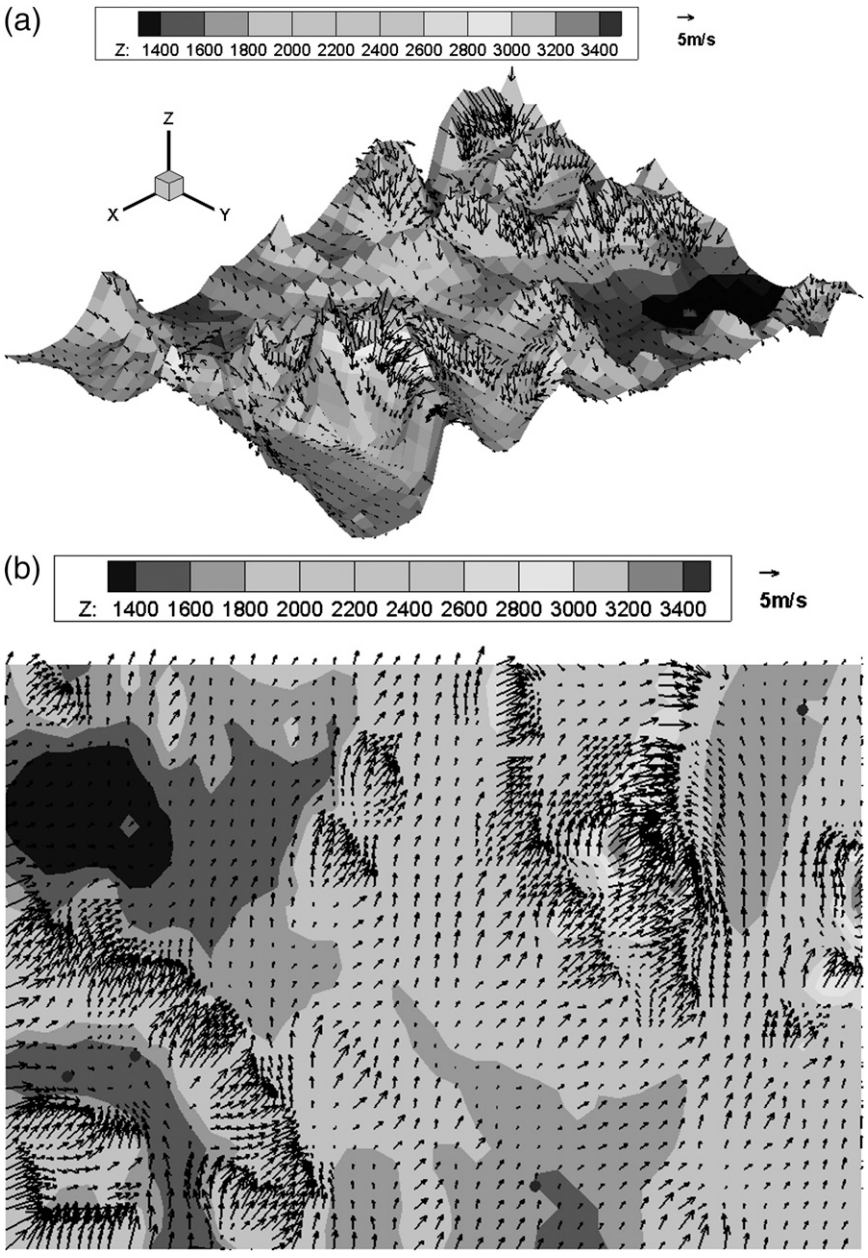

FIG. 15. As in Fig. 14, but with adaptation.

fine mesh is 750 m. The total velocity was chosen as the key variable in the adaptation procedure. Both 2D and 3D views for the adaptive meshes are shown in Fig. 13. Notice that the meshes are especially refined at regions where topography changes abruptly, which is usually attributed to rapidly changing wind speeds with large computational errors.

Both 2D and 3D views of wind fields from MM5 are shown in Fig. 14. The adaptive wind field results are shown in Fig. 15.

A comparison of the 100-m layer winds is shown in Fig. 16. The overall differences in both velocity magnitude and directions are within 5%. However, an added benefit in using *h*-adaptation is that much higher resolution can be obtained, especially where the terrain is highly irregular and frequently changing over a wide expanse. The ability to obtain a more accurate 3D wind field representation greatly assists in producing a more accurate wind power density map and potential placement of wind turbines.

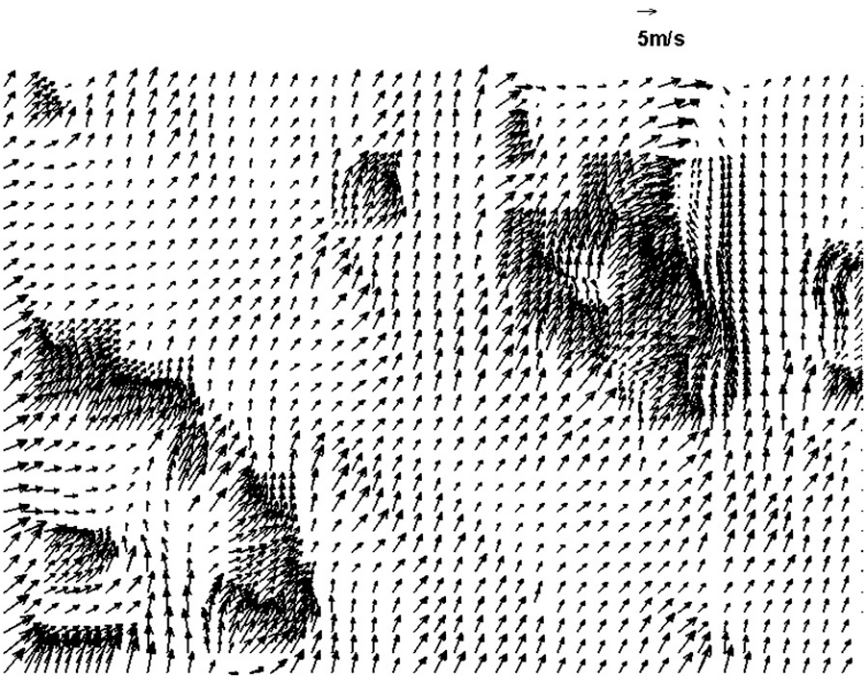

FIG. 16. Difference between 100-m wind fields from MM5 and adaptive FEM for central Nevada.

5. Conclusions

An *h*-adaptive mass-consistent FEM has been developed for constructing 3D wind fields utilizing a Sasaki variational approach. The algorithm refines and unrefines meshes automatically based on velocity and/or topographical features. Adaptive wind fields are presented for both the Nevada Test Site and a central region within Nevada under investigation for potential wind energy generation. Model results obtained with the adaptive model were in good agreement with field data and MM5 results. The application of an *h*-adaptive technique permits the construction of localized high-resolution wind field estimates in regions where refined mesh resolution is warranted. Such schemes can be effective in contaminant dispersion simulations where there is a need to accurately define locations with high contaminant concentrations. The method is also useful in refining meteorological tower locations and more accurately determining potential wind turbine sites in wind energy assessment studies.

Adaptive FEM algorithms are cost efficient—this is well documented in the literature. The application of *h*-adaptation for meteorological simulations appears promising when dealing with large-scale calculations over regions where localized fine meshing is needed to accurately capture rapidly changing flow features.

Acknowledgments. We thank Dr. Darryl Randerson (retired), NOAA/ARL-SORD, and Dr. David Carrington, LANL, for their assistance and guidance in examining the tower data at the NTS. We also thank Dr. Darko Koracin and Dr. Richard Reinhardt at the Desert Research Institute, Reno, NV, for their help in examining the tower data from the four towers and results from the MM5 simulations. We are thankful to NREL for its support and financial assistance in the wind energy assessment effort.

REFERENCES

Ainsworth, M., and J. T. Oden, 2000: *A Posteriori Error Estimation in Finite Element Analysis*. Pure and Applied Mathematics, Series of Texts, Monographs and Tracts, Wiley-Interscience, 264 pp.

Biswas, R., and R. C. Strawn, 1998: Tetrahedral and hexahedral mesh adaptation for CFD problems. *Appl. Numer. Math,* **26,** 135–151.

Demkowicz, L., 2006: *Computing with hp-Adaptive Finite Elements.* Vols. 1 and 2, *Dimensional Elliptic and Maxwell Problems,* CRC Press, 398 pp.

——, J. T. Oden, W. Rachowicz, and O. Hardy, 1989: Toward a universal *h-p* adaptive finite element strategy, Part 1. Constrained approximation and data structures. *Comput. Methods Appl. Mech. Eng.,* **77,** 79–112.

Dickerson, M. H., 1978: MASCON-A mass consistent atmospheric flux model for regions with complex terrain. *J. Appl. Meteor.,* **17,** 241–253.

Finardi, S., G. Tinarelli, P. Faggian, and G. Brusasca, 1998: Evaluation of different wind field modeling techniques for wind energy applications over complex topography. *J. Wind Eng. Ind. Aerodyn.,* **74–76,** 283–294.

Goodin, W. R., G. J. Mcrae, and J. H. Seinfeld, 1979: A comparison of interpolation methods for sparse data: Application to wind and concentration fields. *J. Appl. Meteor.,* **18,** 761–771.

——, ——, and ——, 1980: An objective analysis technique for constructing three-dimensional urban-scale wind fields. *J. Appl. Meteor.,* **19,** 98–108.

Guo, B., and I. Babuska, 1986a: The *h-p* version of the finite element method—Part 1: The basic approximation results. *Comput. Mech,* **1,** 21–41.

——, and ——, 1986b: *The h-p* version of the finite element method—Part 2: General results and applications *Comput. Mech*., **1,** 203–220.

Heinrich, J. C., and D. W. Pepper, 1999: *Intermediate Finite Element Method: Fluid Flow and Heat Transfer Applications.* Taylor and Francis, 600 pp.

Kitada, T., A. Kaki, H. Ueda, and L. K. Peters, 1983: Estimation of vertical air motion from limited horizontal wind data-A numerical experiment. *Atmos. Environ.,* **17,** 2181–2192.

Lange, R., 1978: A three-dimensional transport-diffusion model for the dispersal of atmospheric pollutants and its validation against regional tracer studies. *J. Appl. Meteor.,* **17,** 241–256.

Mathur, R., and L. K. Peters, 1990: Adjustment of wind fields for application in air pollution modeling. *Atmos. Environ.,* **24,** 1095–1106.

Montero, G., and N. Sanin, 2001: 3-D modeling of wind field adjustment using finite differences in a terrain conformal coordinate system. *J. Wind Eng. Ind. Aerodyn.,* **89,** 471–488.

——, E. Rodríguez, R. Montenegro, J. M. Escobar, and J. M. González-Yuste, 2005: Genetic algorithms for an improved parameter estimation with local refinement of tetrahedral meshes in a wind model. *Adv. Eng. Software,* **36,** 3–10.

Nithiarasu, P., and O. C. Zienkiewicz, 2000: Adaptive mesh generation for fluid mechanics problems. *Int. J. Numer. Methods Eng.,* **47,** 629–662.

Oñate, E., and G. Bugeda, 1994: Mesh optimality criteria for adaptive finite element computations. *The Mathematics of Finite Elements and Applications: Highlights 1993*, J. R. Whiteman, Ed., John Wiley and Sons, 121–135.

Pepper, D. W., 1991: A finite element model for calculating 3-d wind fields over Vandenberg Air Force Base. *29th AIAA Aerospace Sciences Meeting*, AIAA Paper 91-0451, Reno, NV, American Institute of Aeronautics and Astronautics, 1–8.

——, and D. E. Stephenson, 1995: An adaptive finite element model for calculating subsurface transport of contaminant. *Ground Water,* **33,** 486–496.

——, and D. B. Carrington, 1999: Application of *h*-adaptation for environmental fluid flow and species transport. *Int. J. Numer. Methods Fluids,* **31,** 275–283.

——, and J. C. Heinrich, 2006: *The Finite Element Method: Basic Concepts and Applications.* 2nd ed. Taylor and Francis, 312 pp.

——, and X. Wang, 2007: Application of an *h*-adaptive FEM for wind energy assessment in Nevada. *Renewable Energy,* **32,** 1705–1722.

Pielke, R., 1984: *Mesoscale Meteorological Modeling.* Academic Press, 612 pp.

Ratto, C. F., R. Festa, C. Romeo, O. A. Frumento, and M. Galluzzi, 1994: Mass-consistent models for wind fields over complex terrain: The state of the art. *Environ. Software,* **9,** 247–268.

Sasaki, Y., 1958: An objective analysis based on the variational method. *J. Meteor. Soc. Japan,* **36,** 77–88.

Schaefer, J. T., and C. A. Doswell III, 1979: On the interpolation of a vector field. *Mon. Wea. Rev.,* **107,** 458–476.

Sherman, C. A., 1978: A mass-consistent model for wind field over complex terrain. *J. Appl. Meteor.,* **17,** 312–319.

Wang, X., and D. W. Pepper, 2007a: Application of an *hp*-adaptive FEM for solving thermal flow problems. *AIAA J. Thermophys. Heat Transfer,* **21,** 190–198.

——, and ——, 2007b: Application of *h-, p-* and *hp*-adaptation for convection heat transfer problems. *45th AIAA Aerospace Sciences Meeting*, Reno, NV, American Institute of Aeronautics and Astronautics, 9792–9800.

Warner, T. T., R. R. Fizz, and N. L. Seaman, 1983: A comparison of two types of atmospheric transport models—Use of observed winds versus dynamically predicted winds. *J. Climate Appl. Meteor.,* **22,** 394–406.

Winter, G., G. Montero, L. Ferragut, and R. Montenegro, 1995: Adaptive strategies using standard and mixed finite elements for wind field adjustment. *Sol. Energy,* **54,** 49–56.

Zienkiewicz, O. C., and R. J. Z. Zhu, 1987: A simple error estimator and adaptive procedure for practical engineering analysis. *Int. J. Numer. Methods Eng.,* **24,** 337–357.